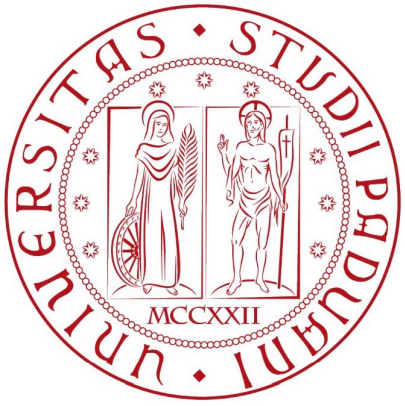

UNIVERSITÀ DEGLI STUDI DI PADOVA

Dipartimento di Fisica e Astronomia
Corso di Laurea Triennale in Fisica

Performance of a shower front detector at high altitudes in the South American Andes

Relatore:
Prof. Michele Doro

Correlatori:
Dott. Cornelia Arcaro
Dott. Tommaso Dorigo

Candidato:
Tommaso Guercio

ANNO ACCADEMICO 2021/2022

Contents

List of Figures

Il Southern Wide-field Gamma-ray Observatory (SWGO) sarà il primo shower-front detector ad osservare un'ampia porzione del cielo meridionale. Il progetto prevede la costruzione di un array di detector distribuiti su un'area di circa 300'000 m^2 in Sud America, nelle Ande, che rileveranno gli sciami atmosferici prodotti dai raggi gamma. L'enorme quantità di segnale di background causato dai raggi cosmici rappresenta però un ostacolo per le misurazioni che deve essere preso in considerazione. Questa tesi si propone quindi di investigare le differenze principali tra il segnale dei raggi gamma e quello di disturbo, analizzando simulazioni di sciami atmosferici generati da raggi gamma e protoni. L'analisi si basa sullo studio delle distribuzioni a terra delle particelle, e mostra come sia di fondamentale importanza il tracciamento dei muoni, per poter confrontare la densità di queste particelle nei due casi e riuscire a distinguere il background. Viene poi mostrata l'importanza di considerare anche altri elementi caratteristici delle cascate, per non incorrere in errori di identificazione, e infine vengono presentati dei possibili sviluppi futuri per ottenere una migliore selezione del segnale.

The Southern Wide-field Gamma-ray Observatory (SWGO) will be the first shower-front detector to observe a large portion of the southern sky. The project involves the construction of an array of detectors distributed over an area of approximately 300'000 m^2 in the South American Andes, which will detect air showers produced by gamma rays. However, the enormous amount of background signal caused by cosmic rays represents an obstacle to the measurements that must be taken into consideration. This thesis therefore aims to investigate the main differences between the gamma-ray signal and the disturbance signal, analyzing simulations of air showers generated by gamma rays and protons. The analysis is based on the study of particles ground distributions, and shows how the tracking of muons is of fundamental importance, in order to compare the density of these particles in the two cases and be able to distinguish the background. The importance of considering also other characteristic elements of the cascades is then shown, in order not to incur identification errors, and finally possible future developments to obtain a better signal selection are presented.

1. Introduction

The Southern Wide-field Gamma-ray Observatory (SWGO) is a gamma-ray observatory to be constructed in South America. It is designed to detect air shower particles initiated by gamma-rays entering the Earth's atmosphere.

The SWGO Collaboration was founded in July 2019 by a group of about 40 institutions from 9 countries as an international R&D Project to develop what would be the first shower-front detector for TeV gamma-ray astronomy above 100 TeV in the Southern Hemisphere . The baseline design constitutes of water Cherenkov detector units to sample the gamma ray-induced particle showers in the atmosphere, by measuring the light produced when the shower particles cross the water tanks. [SWG22] The light produced, called Cherenkov radiation, is emitted when a charged particle passes through a dielectric medium at a speed greater than the phase velocity of light in that medium.

The new observatory is planned to be installed in the Andes, at or above 4.4 km a.s.l., as high altitude is crucial for pushing the energy threshold down to 100 GeV range [Sin09]. At the highest energy range the goal is to reach a good sensitivity to gamma rays beyond 100 TeV, in order to detect PeVatrons (which will be discussed below).

The current detector configuration plan consists in the combination of a high fill-factor core of circa 80,000 m^2 with instrumented area above 80%, and a significantly larger and sparse outer array of at least 200,000 m^2, to provide at one time a low energy detection threshold and good sensitivity to high-energy events. [Alm21]

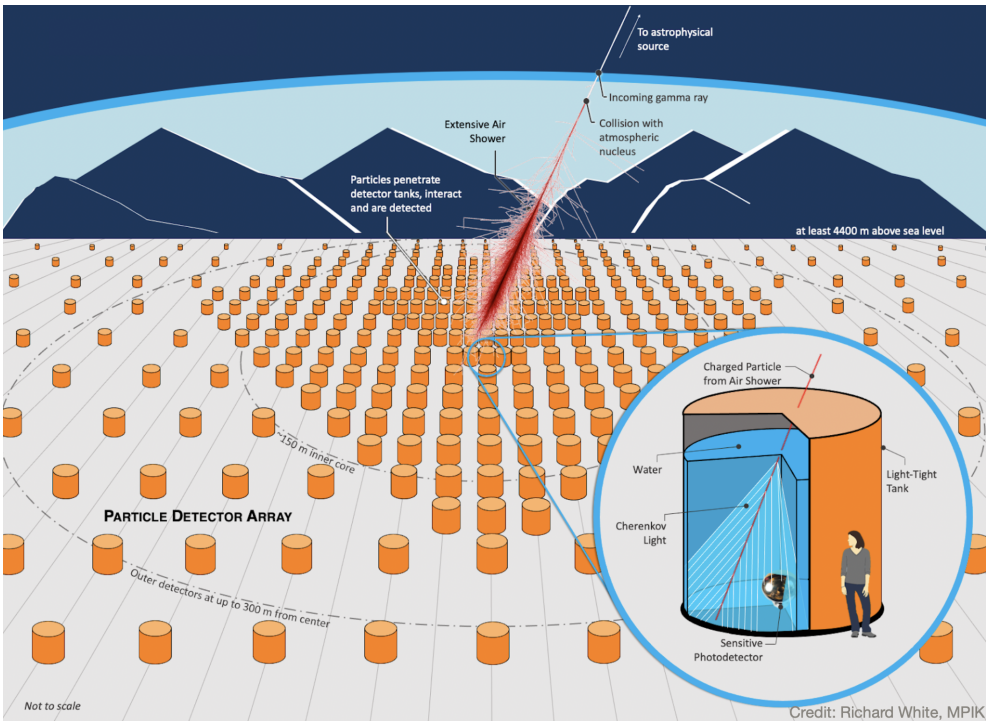

Figure 1.1: Graphical representation of SWGO's detectors spacial disposition

The primary detector technology options for the water Cherenkov detector units of SWGO are (see Figure 1.2):

- Tanks: individual detector units mechanically separated and individually deployed, with light tight liners

within roto-moulded plastic or steel tanks.

- Ponds: four or more large artificial water volumes with retaining walls and optical separation between units.
- Lake: deployment of detector unit bladders filled with pure water directly in to a natural lake. [Hin21]

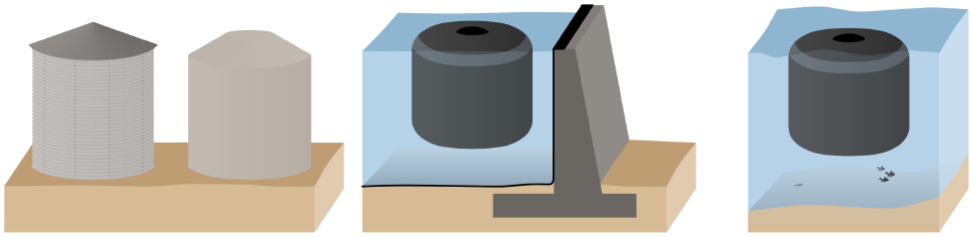

Figure 1.2: Detector concepts under study

SWGO's main scientific objectives are high energy astrophysics searches, with a special focus on gamma-rays composition and anisotropy, dark matter, and galactic accelerators. The interest in studying gamma rays resides in the fact that, unlike all the cosmic rays that constantly hit the earth atmosphere, this radiations provide information about their origin. Gamma rays travel undeflected through space from their place of production, whereas cosmic rays, being charged, are deflected by cosmic magnetic fields and arrive almost isotropically to the earth.

Gamma rays can be produced in various ways, e.g., in interactions between TeV electrons or super-PeV protons and local strong magnetic fields leading to synchrotron emissions, inverse Compton scattering of GeV-TeV electrons on soft photon fields, Bremsstrahlung of electrons and protons intersecting a high dense region of plasma or gas, electron-positron annihilation, or decay of energetic neutral pions. Gamma rays are always produced where high energy cosmic-rays are accelerated, therefore they can be studied to gain informations about the cosmic accelerators that are able to speed up particles up to almost the speed of light. [Dor09]

The Cosmic-ray factories that accelerate particles to PeV energies are called PeVatrons. Some of the possible galactic sources of very high-energy particles are pulsars, pulsar wind nebulae, supernova remnants, and young massive star clusters, while some extragalactic sources are blazars and starburst galaxies. Their principal signature is ultra-high-energy (exceeding 100 TeV) gamma radiation. Detecting gamma rays is however a hard task: since they cannot be focused by conventional telescope techniques, i.e. lenses and mirrors, due to the nuclear interactions they manifest with matter, they can only be observed indirectly and subsequently reconstructed. This can be done with satellite-based detectors or ground-based detectors, but for energies above 100 TeV the fluxes become so low that it is impossible to perform measurements by means of the small area detectors that can operate on satellites. To find enough high energy gamma radiations it is necessary to rely on observatories with a vast area filled with detectors, i.e., extensive air-shower arrays (EASs). EASs perform measurements on cascades produced by gamma rays in the atmosphere. The process leading to the generation of these electromagnetic showers can be summarized as follows: the interaction between the gamma ray and the electric field of atmospheric molecules induces pair-production of an electron-positron pair:

$$\gamma(\gamma) \rightarrow e^{+}e^{-} \tag{1.1}$$

Electrons and positrons in turn generate new gamma rays via bremsstrahlung:

$$e^{\pm}(\gamma) \rightarrow e^{\pm}\gamma \tag{1.2}$$

Eventually the secondary gamma ray again pair-produces an electron and a positron and so on, redistributing the energy between the particles produced, until particle energy reaches a threshold value below which ionization takes over. At this point all the particles produced make collisions of other kinds and the shower rapidly dies out.

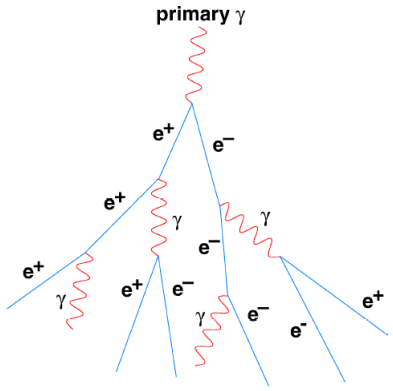

Figure 1.3: Schematic representation of an air shower initiated by a gamma-ray (from [AMP08])

The flux of gamma rays that hit the atmosphere is however much lower than the flux of cosmic rays, therefore among all the events detected by the ground detectors it is necessary to distinguish the background given by hadronic showers. This type of cascades are initiated by the strong interaction between the hadrons and the atmospheric nuclei, leading to the production of pions, kaons, and nucleons. Neutral pions π^0 decay into pairs of photons:

$$\pi^0 \rightarrow \gamma\gamma \tag{1.3}$$

The photons produced form an electromagnetic cascade. Charged pions $\pi^{\pm}$ almost always decay into muons and (anti)neutrinos:

$$\pi^+ \rightarrow \mu^+\nu_\mu \qquad\qquad \pi^- \rightarrow \mu^-\bar{\nu}_\mu \tag{1.4}$$

This is how the muons and neutrinos that eventually reach the ground are produced in the air shower. Due to their large lifetime, muons can travel relevant portion of the atmosphere and carry far from the initial hadron track a substantial part of its energy. As a result, the hadronic shower is way broader compared to an electromagnetic shower. [Dor09]

Just like charged pions, kaons can produce muons in the process, but can also decay into pions:

$$K^+ \rightarrow \mu^+\nu_\mu \qquad\qquad K^- \rightarrow \mu^-\bar{\nu}_\mu \qquad\qquad K^{\pm} \rightarrow \pi^{\pm}\pi^0 \tag{1.5}$$

Pions, kaons, and heavy baryons are unstable and decay into lighter and more stable particles relatively high in the atmosphere, and in particular neutral pions decay into pairs of photons, which produce electromagnetic cascades. For this reason the particles that manage to reach the ground are about the same as the ones in electromagnetic showers. Being able to distinguish hadron showers from electromagnetic showers can be therefore a particularly difficult but crucial task for ground based detectors.

Background rejection is indeed a central performance driver for SWGO. A long-established discriminant between gamma and background showers is muon content, and the power of this approach has recently been demonstrated by the observatory LHAASO [Aha+21]. Two different approaches are being pursued in SWGO to tag muons passing through individual detector units: a double layer approach [Kun21] and multiple-PMTs in a single shallow layer [Con+21].

The double layer approach takes advantage of a horizontal separator that stops the Cherenkov light generated by the electrons in the upper room while grants that the light generated in the lower room is solely generated by muons. Consequently, a signal detected in the lower layer reveals the passage of a muon. On the other hand using multiple photosensors facing upward at the bottom of the tank allows to discern muons from electrons and photons thanks to the photon signal asymmetry between the sensors, which is larger for muons.

One of the EASs currently in operation that can be taken as an example for the implementation of SWGO is the above-mentioned Large High Altitude Air Shower Observatory (LHAASO). This observatory has found 12 ultra-high-energy (UHE) cosmic accelerators within the Milky Way. It has also detected photons with energies exceeding 1 PeV, including one at 1.4 PeV. The latter is the highest energy photon ever observed. Despite having several potential counterparts in their proximity, including pulsar wind nebulae, supernova remnants, and star-forming regions, the PeVatrons responsible for the ultrahigh-energy gamma rays have not yet been firmly localized and identified (except for the Crab Nebula), leaving open the origin of these extreme accelerators. [Cao+21]

1.1 Methodology

This thesis reports the analysis and discussion of air showers simulations, and its main goal is to provide strategies to discern charged cosmic ray showers background from signal.

Cosmic rays are much more frequent than gamma rays: for each gamma ray, about 1000 cosmic rays are observed [Dor09], and about 90 % of cosmic rays are protons, so the discussion below focuses on the comparison between gamma and proton showers.

The data were obtained thanks to CORSIKA, a detailed Monte Carlo program to study the evolution of Air Showers in the atmosphere initiated by photons, protons, nuclei, or any other particle. The particles are tracked through the atmosphere until they experience reactions with the air nuclei or decay.

Thousands of events generated by protons and gamma rays at different energies have been simulated. The analysis was then focused on a series of fixed energies (1 TeV, 10 TeV, 100 TeV, 1 PeV and 10 PeV) and a comparison was made between gamma and proton events at these energies. It is important to underline that the proton events were not simulated by fixing a specific energy value, but a wide interval, in order to have a generic variety of background events. To carry out this analysis, however, only the events with energy close to the desired ones were selected in order to make a direct comparison with the respective gamma events. The only energy value that has been set for proton cascades is 100 TeV. Finally the low energy events (between 1 and 10 TeV) were simulated in a wide interval for both gamma and proton events.

Various graphs have been generated and analyzed to make these comparisons, e.g.:

- Ground pattern

- Lateral distribution
- Time profile

A selection was then made on proton air showers to focus attention on the events more difficult to distinguish with respect to the signal: muon-starved events, i.e. proton showers with a reduced number of muons compared to the average. Given that the main characteristic that allows to distinguish hadronic showers from electromagnetic ones is the number of muons (much greater for hadron showers), muon-starved events are a considerable obstacle for the search for the gamma-ray signal.

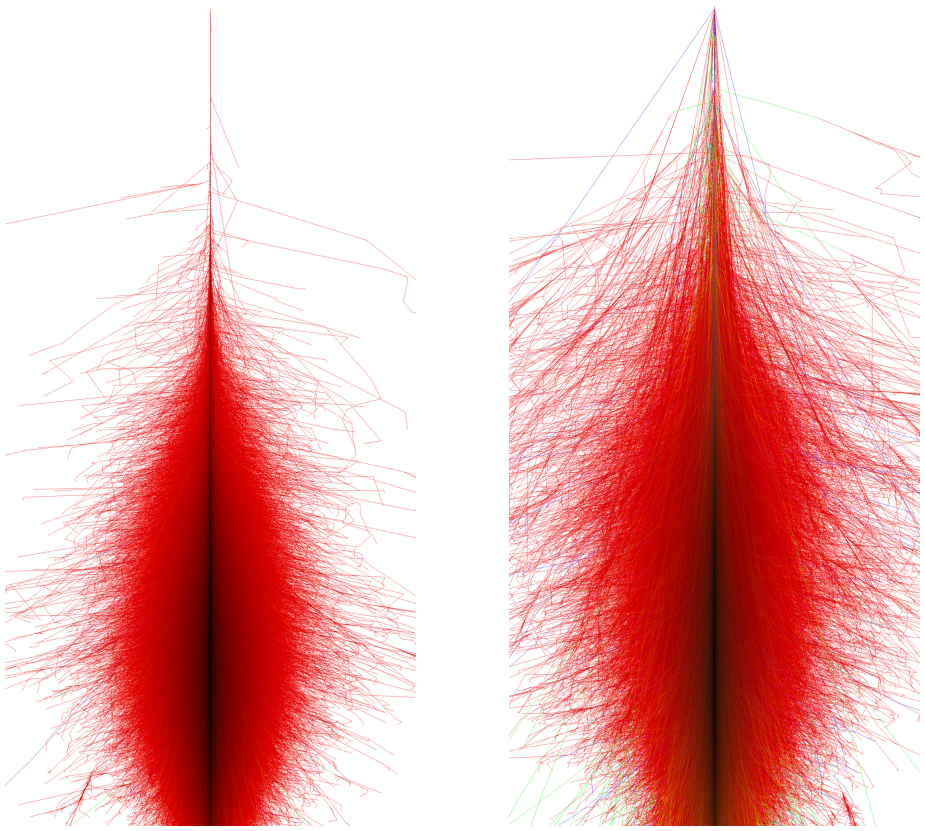

Figure 1.4: CORSIKA Simulations of two air showers initiated by a photon (left) and a proton (right) with initial energy of 100 TeV. (From the CORSIKA website [Hec])

2. Data Analysis and results

One of the projects utilized by the SWGO Collaboration concern a software capable of facilitating the analysis of simulated data and the generation of graphs useful for the development and design of the future observatory. The scripts written for this thesis will be able to contribute to this project.

The analysis of CORSIKA files was done through Python scripts, and a python module to read the CORSIKA binary output files named `pycorsikaio` [Noe] was used to access the data.

The first approach to the air showers analysis was the study of ground pattern graphs for gamma and proton events at different energies. Figure 2.1 shows the coordinates of the particles that have reached the ground, taking the position of the shower core as the origin of the axes.

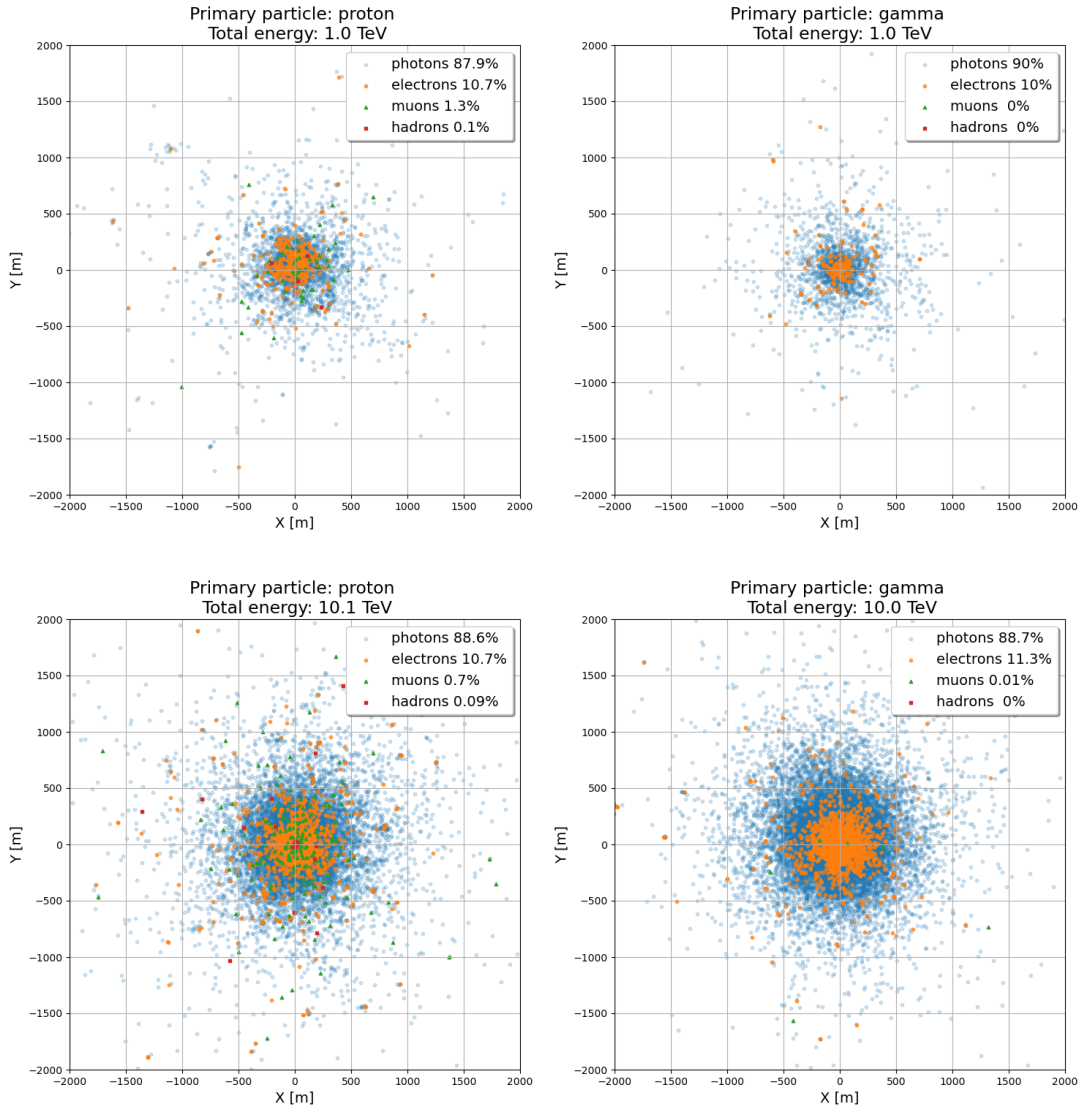

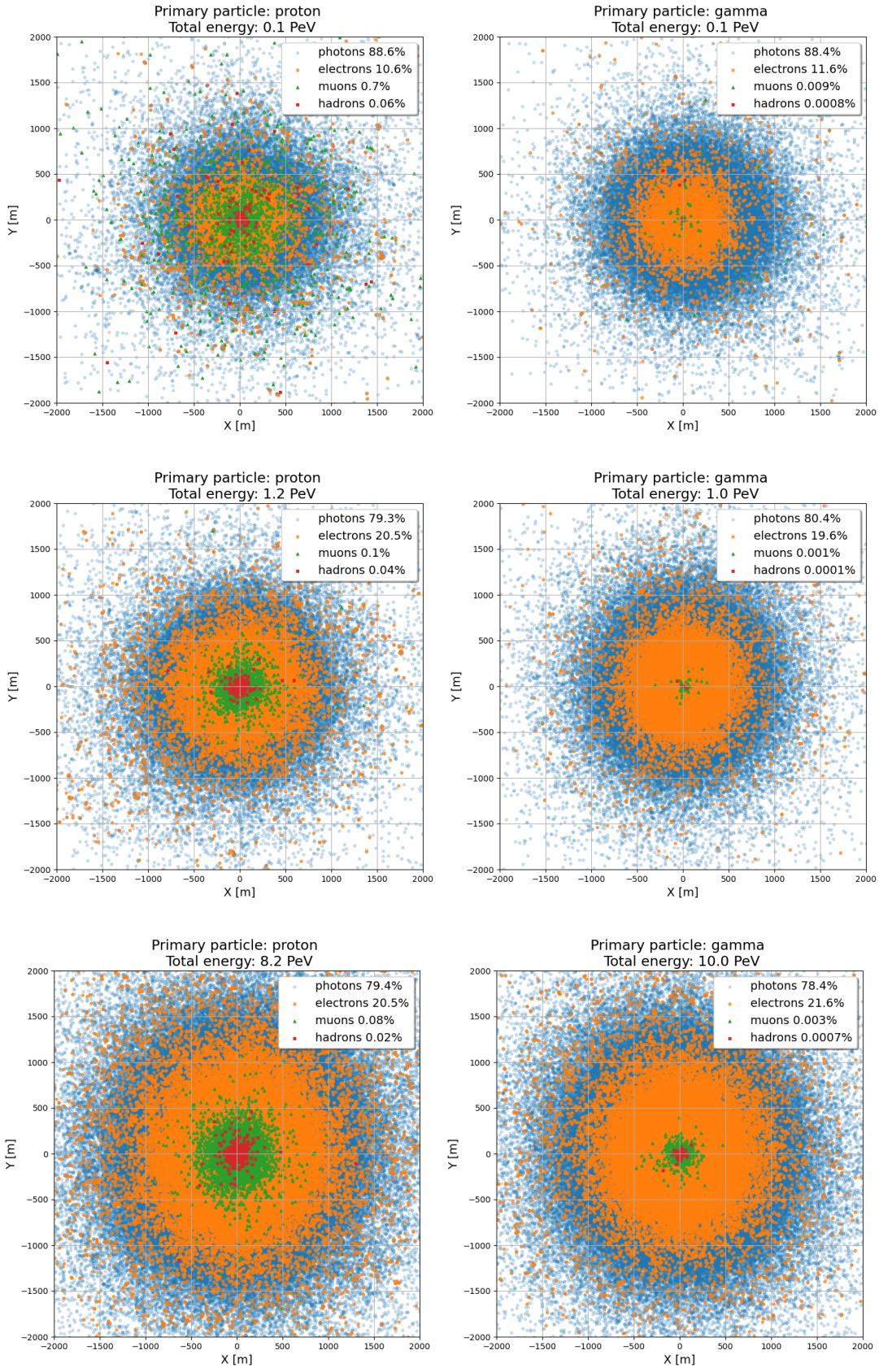

Figure 2.1: Comparison of proton and gamma ground pattern graphs at different energies

It is clearly visible from figure 2.1 that the shower radius and number of particles increases as the energy gets higher. This happens because the showers generated by high-energy primary particles reach later the threshold energy that stops the cascade, so more particles are produced and distributed over a larger area.

It is also noticeable that proton showers are slightly broader than gamma-rays ones, for the reasons explained in the introduction.

One element that may seem unexpected in figure 2.1 is the presence of muons in electromagnetic showers. These particles can be generated from photons by pair production, but the cross section for muon-antimuon pair production is many orders of magnitude smaller than the electron-positron one, due to its larger mass. This phenomenon therefore rarely happens, and becomes noteworthy only for high energies. Another mechanism that has to be taken into account is the electron–positron annihilation into hadrons. The positrons from the initial gamma-ray pair production have a considerable probability of generating hadrons hitting an electron of an atom in the atmosphere. This process could explain the presence of hadrons in the highly energetic gamma cascades. It also contribute to the production of muons because hadron such as kaons and pions can decay into these types of leptons.

The main difference between gamma and proton graphs lies in the number of muons and hadrons. From the legend of the graphs it can be seen that the percentage of these types of particles is much higher in proton cascades, just as one would expect.

As explained in the introduction, SWGO will be equipped with muon detectors to be able to discriminate background events. However, it must be taken into account that it is not enough to know only the number of muons, because otherwise one could mistake a high-energy gamma cascade for a low-energy proton cascade for example, since they could have a similar number of muons. Another error can arise when a proton event with a lower than average number of muons, called muon-starved, is detected: it can easily be confused with a gamma event. Some strategies used to try to distinguish these types of events will be discussed below.

Another type of graph useful for analyzing simulated air showers is the lateral distribution. This graph shows the particle density as a function of the distance from the shower core. To calculate the particle density, the number of particles N contained in a circular crown centered in the core was divided by the value of this area. The annulus in this formula has an inner radius r and an outer radius $r+dr$:

$$\rho(r) = \frac{N}{\pi(dr^2 + 2rdr)} \tag{2.1}$$

The curves were obtained by defining a spatial range between 0 and 1500 meters to be divided into a certain number of intervals, called bins, which were filled whenever the distance of a particle from the center belonged to that range. The bin counts were then divided by the corresponding annulus area to obtain the particle density.

The top row of Figures 2.2 and 2.3 shows the lateral distributions for protons and gammas respectively. In each of these graphs the averages on all the events taken into consideration of photons, electrons and muons are shown. The curves of each single event were instead printed in transparency to give an idea of the data fluctuation. In some graphs it can be seen that the averages do not follow the trend of the curves of the single events. This is due to the fact that in these graphs many of the single event curves have several empty bins, and therefore lower the average value in those points. This happens in fact in the muon curves for gamma events, which have a limited number of muons, and for the 1 TeV curves, which have few particles in general since they are low energy events.

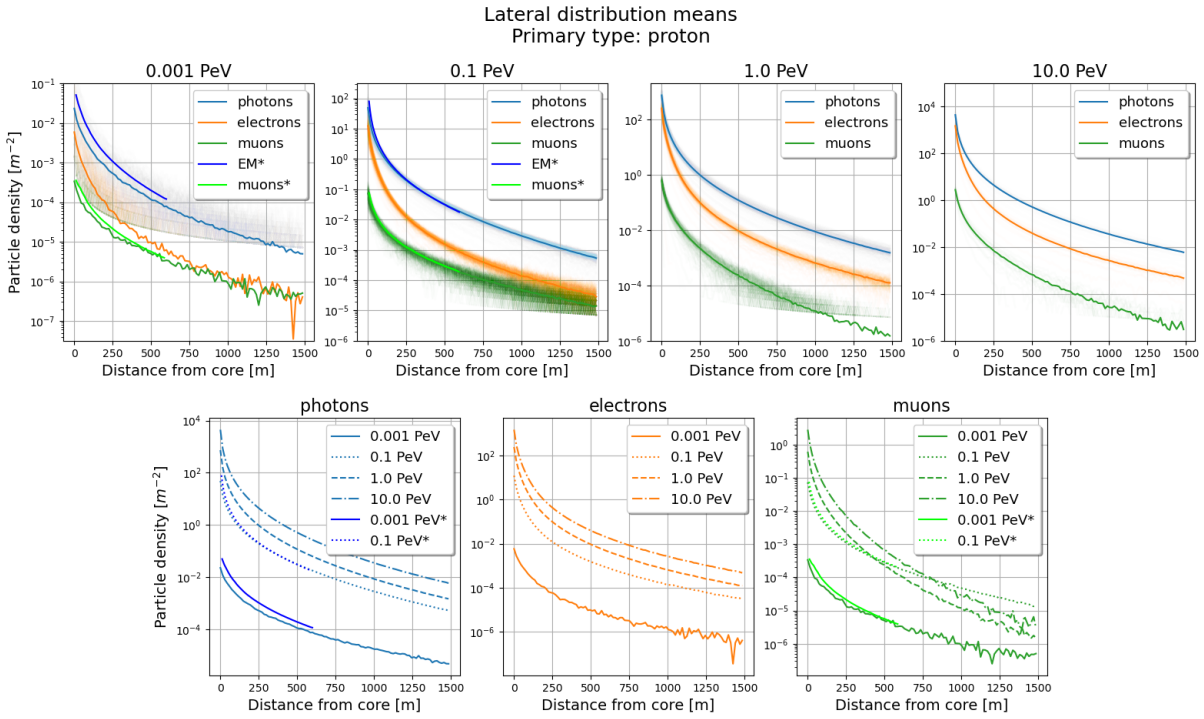

Figure 2.2: Lateral distribution for showers initiated by protons with initial energy of 1 TeV, 100 TeV, 1 PeV and 10 PeV. The data marked with an asterisk in the legend are taken from [PS19]

The lower line instead shows a comparison between the averages of the lateral distributions at different energies for the particles under examination.

The graphs show how the density at the core is very high, then it falls very quickly in the first 100 meters or so and finally continues to drop but less steeply. Near the core it can be seen that the density of electrons is slightly lower than that of photons. However, with increasing distance the electron density drops much faster than the photonic one. Photons are therefore more evenly distributed in the impact area than electrons. The muon density is lower compared to others from the beginning, but in the 1 PeV and 10 PeV graphs it also drops faster than that of photons and electrons. This shows that the muons at these energies are all concentrated around the core. For the cascades at 1 TeV and 100 TeV, the density of muons instead decreases slower than that of photons and electrons. This is unexpected, also because as can be seen from the graphs at the bottom right of figures 2.2 and 2.3, the density of the muons at 100 TeV exceeds that of the curves at 1 PeV and 10 PeV from a certain distance onwards. A possible explanation comes from the fact that muons in the cascades with energy beyond 1 PeV are highly energetic and therefore are deviated less by the Earth's magnetic field and by collisions that can move them away from the core[1]. The less energetic muons of the cascades with energy below 100 TeV are instead deflected more and therefore are distributed over a greater area when they reach the ground. However, this effect may be an artifact as this analysis is still at a preliminary stage.

The graphs in figure 2.2 were also compared with the curves presented in the research paper [PS19] to verify the

[1]We did not have to validate this hypothesis but this is technically possible by setting to zero the magnetic field in the CORSIKA program.

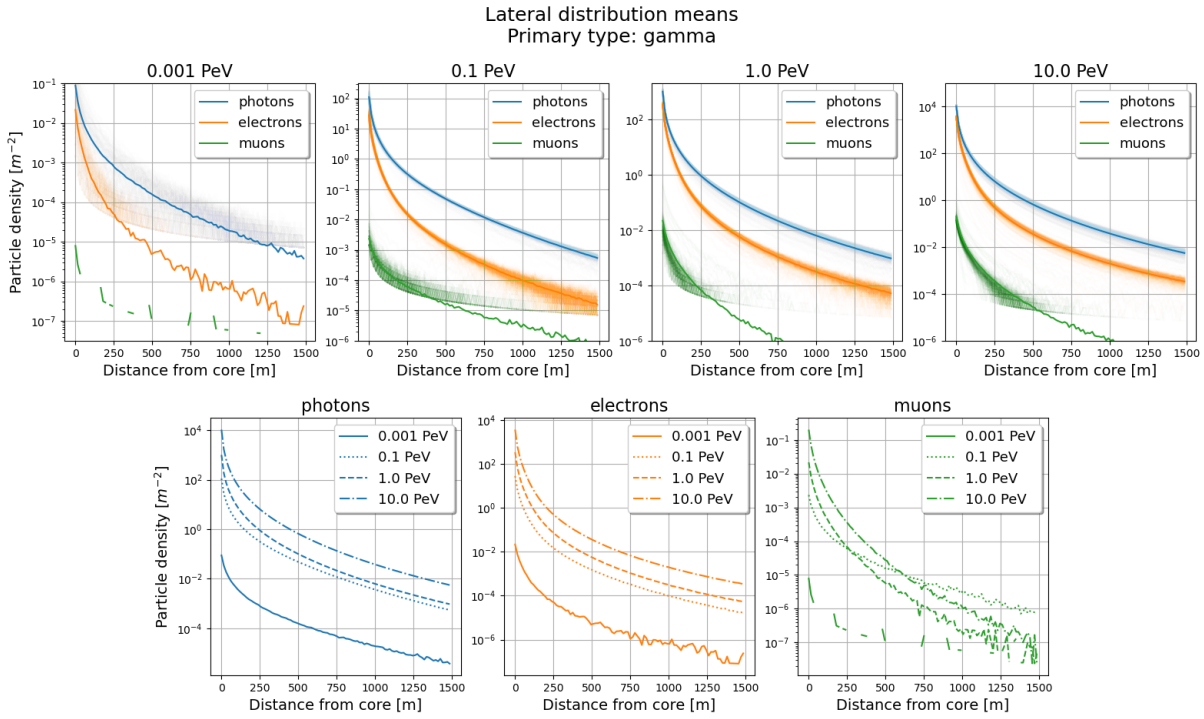

Figure 2.3: Lateral distribution for showers initiated by gamma-rays with initial energy of 1 TeV, 100 TeV, 1 PeV and 10 PeV.

validity of the results obtained. The lateral distributions shown in the article were also obtained from data simulated with CORSIKA so this comparison is appropriate. The curves in the 100 TeV energy graph match perfectly, while in the 1 TeV one they are a bit staggered. This offset may be due to the fact that the data for the 1 TeV curves show greater fluctuations than those at 100 TeV since the events used have an energy within a range of 20 GeV around the chosen value. Despite this there is a very good correspondence with the data of the paper, and this helps to confirm the validity of the results obtained.

Also in this case the main difference between gamma and proton graphs lies in the number of muons, or rather in their density. The muon density in gamma events is about one tenth of that in proton events, and it also tends to decrease faster. This shows that the muons in the gamma cascades are less and more concentrated around the core.

Since the number of muons is not enough as the only discriminant, graphs have been created to show the ratio between the muon curves and the photons or electrons curves. In this way it is possible to take into account more elements and avoid confusing proton and gamma events with a similar number of muons but a large difference in the number of photons and electrons.

From figures 2.4 and 2.5 we can see a clear distinction between the curves with the highest energy (1 PeV and 10 PeV) and the others. In all the graphs the ratios tend to rise in the first few meters, but then only in the ones at 1 TeV and 100 TeV do curves continue to grow, albeit more slowly. In fact, also from figures 2.2 and 2.3 it can be seen that for the first two graphs from the left the distance between the muon curve and the others tends to decrease while in the others it tends to increase.

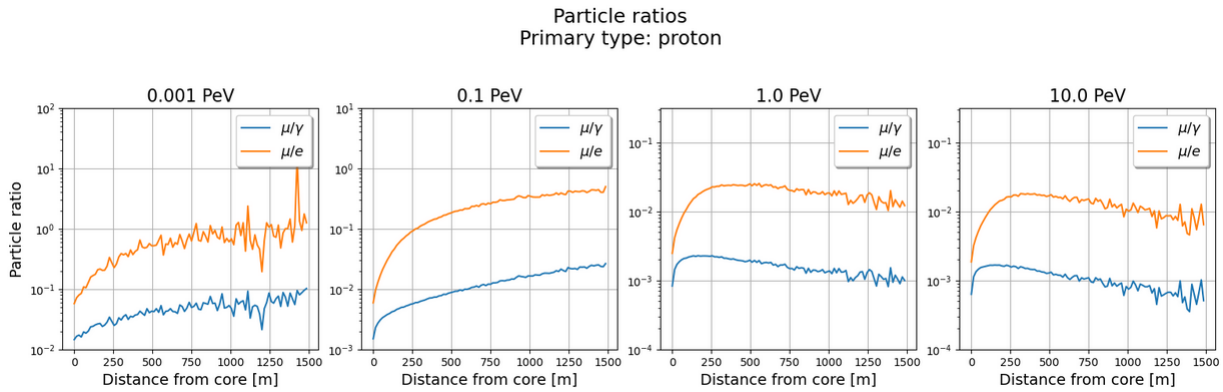

Figure 2.4: Ratio between lateral distribution curves for proton cascades

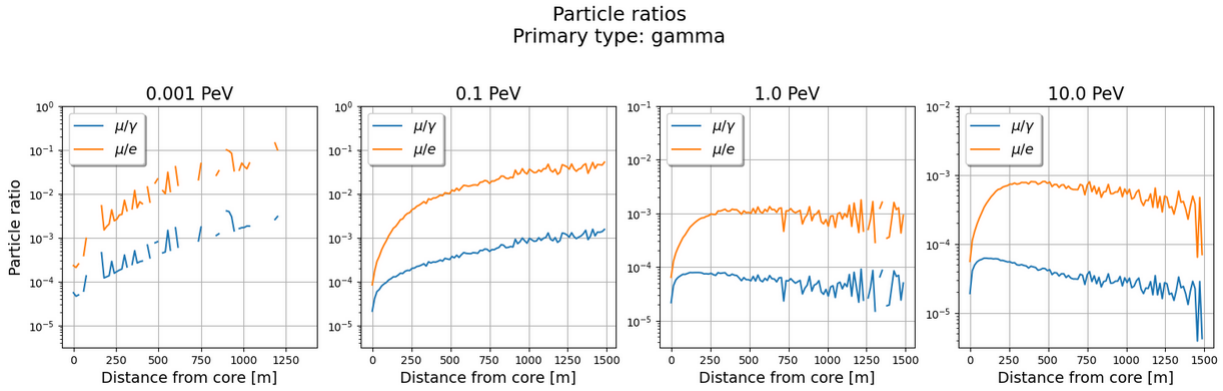

Figure 2.5: Ratio between lateral distribution curves for gamma cascades

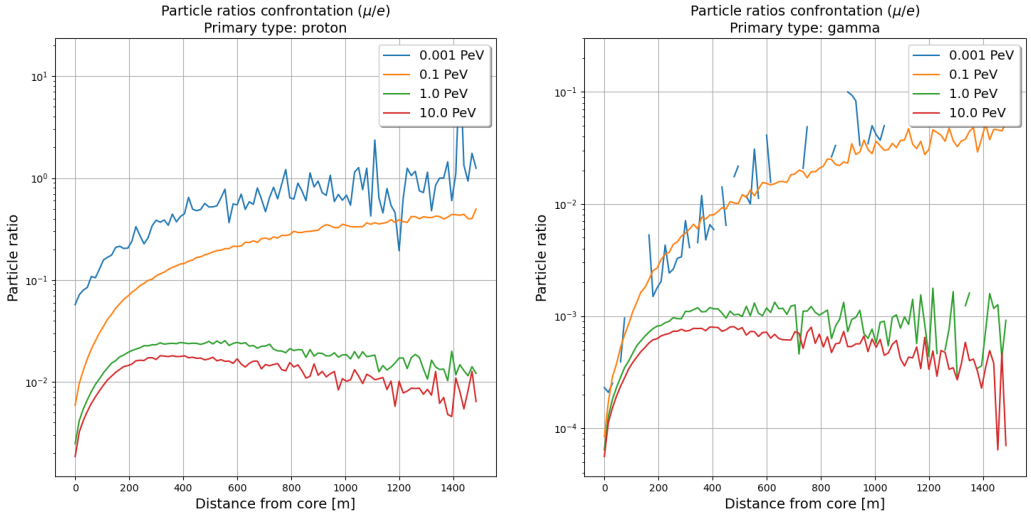

Figure 2.6: Comparison of $\frac{\mu}{e}$ density ratio at different energies

Figure 2.6 shows instead that as the energy increases, the ratios tend to decrease, so at higher energies there are

proportionately fewer muons than those in lower energy events. If the two graphs are compared, it can be seen that the curves have values that differ by many orders of magnitude. The only curves with comparable values are those related to higher energy proton events (1 PeV and 10 PeV) and the ones related to lower energy gamma events (1 TeV and 100 TeV). However, these curves have very different shapes. The former start from a value close to 10^{-4} and go up to 10^{-1}, while the latter are all contained between 10^{-3} and 10^{-2}, and, unlike the others, towards the abscissa value equal to 400 meters they begin to decrease. Since these curves are easily distinguishable from each other, they can be a good starting point for separating the signal from the background.

As mentioned above, the most difficult background events to discriminate are those with a low number of muons, called muon-starved. A minimum threshold of muons was calculated in order to select these types of proton events. To do this, a histogram of the muon counts for each event was created, and from this graph a threshold equal to 3% of the events with the lowest counts was calculated. In figure 2.7, the red bins are those that are below the threshold.

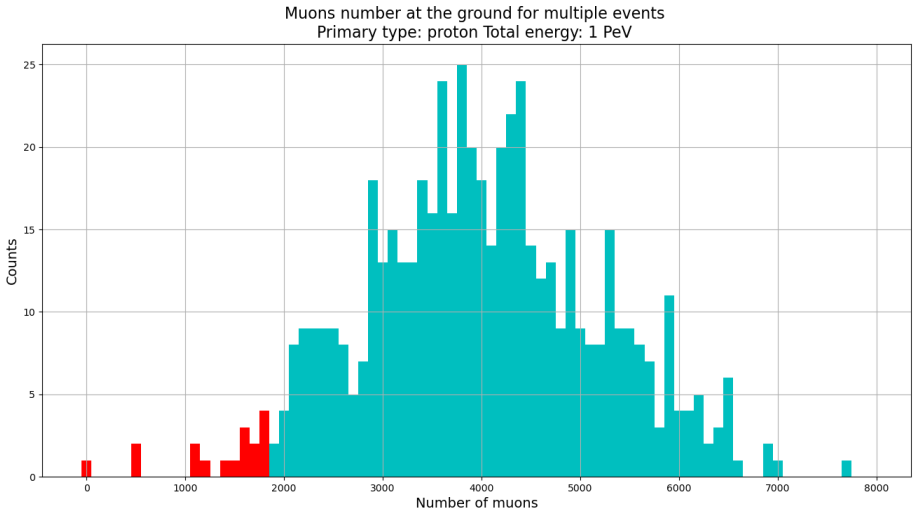

Figure 2.7: Muon number histogram for proton events at 1 PeV. The red section includes events with a number of muons below the 3% threshold

Figure 2.8 shows the lateral distributions for muon-starved events. The 1 TeV graphs have been omitted because they have too small a quantity of particles to be able to make statistics. If we compare these graphs with the proton ones, it can be seen that not only the density of muons is lower, but also of the other particles, so we can say that these events have a smaller quantity of particles than the average. Comparing them instead with the gamma graphs we note that the density of photons and electrons is lower, while the density of muons remains higher, so even if there are much fewer particles than the average, the quantity of muons always remains higher than that of gamma cascades.

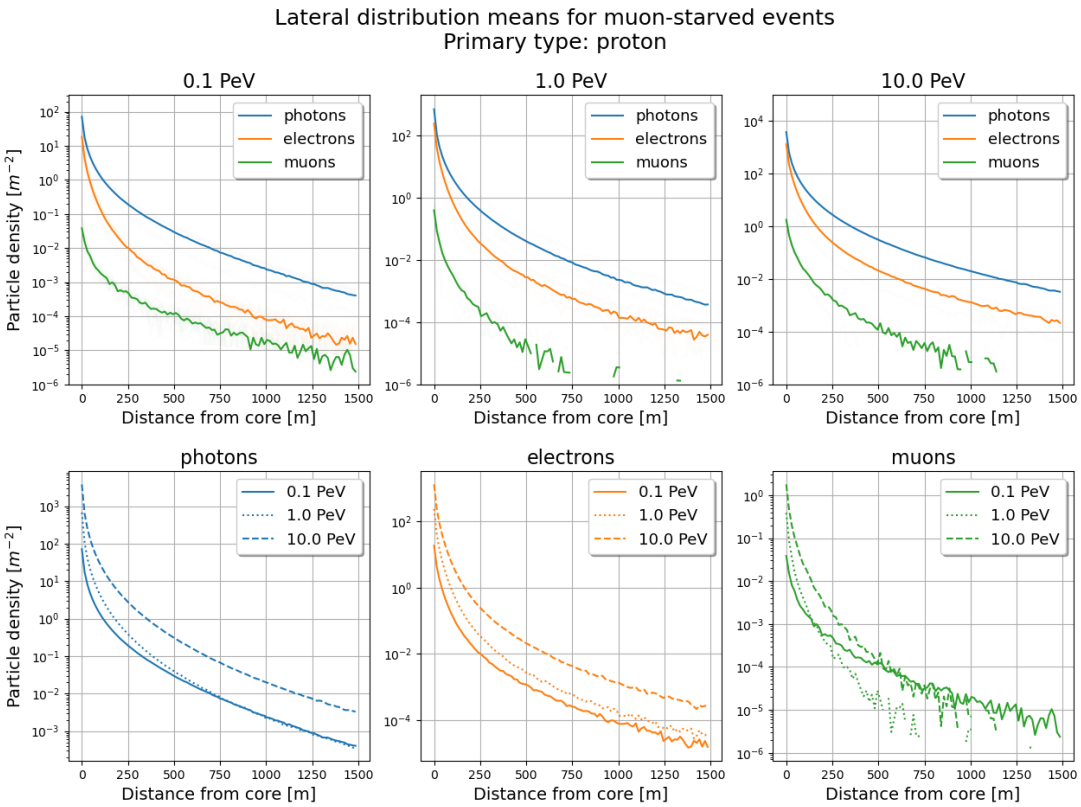

Figure 2.8: Lateral distribution for muon-starved events with primary energy fixed at 100 TeV, 1 PeV and 10 PeV

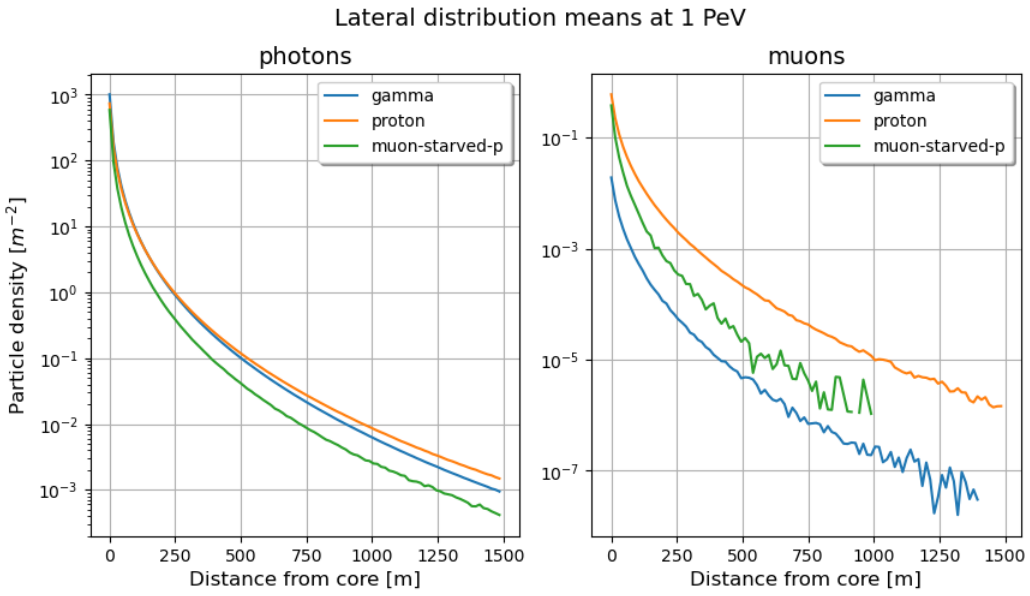

Figure 2.9: Lateral distribution for events at 1 PeV. Comparison between gamma, proton and muon-starved cascades

To better show these considerations, graphs were made with a direct comparison between the proton, gamma, and muon-starved events for the cascades at 1 PeV. From figure 2.9 it can be seen that while the photon density

for gamma and proton events is similar, it is lower for muon-starved events. The fact that the muon density remains instead higher for muon-starved events is a good sign because it means that even in these cases there is a distinction in the number of muons which helps to separate the background from the signal. By exploiting the information obtained on the density of both muons and photons of muon-starved events it should be easier to make this distinction.

Finally, graphs 2.10 and 2.11 have been produced to show the time profile of the cascades at fixed energies. These histograms were made to display the time of arrival to the ground of the particles, setting as the initial instant the moment in which the first interaction of the primary with the atmosphere takes place. In this case no averages were made on multiple events because there was not a good match between the individual cascades since the first interaction occurs at different points every time, and therefore the peaks appeared at different time coordinates for each event. Looking at the time profile of a single cascade, a qualitative analysis can still be made to obtain some informations. From these graphs it can be seen that the peak of the signal arrives at approximately the same instant for all particles. The substantial difference is that the muon signal is shorter than that of photons and electrons. The muon signal is also longer and with more counts in the proton graphs compared to that of gamma graphs, while the other signals are similar in the two cases. After all, time profiles do not seem to provide much help for background separation.

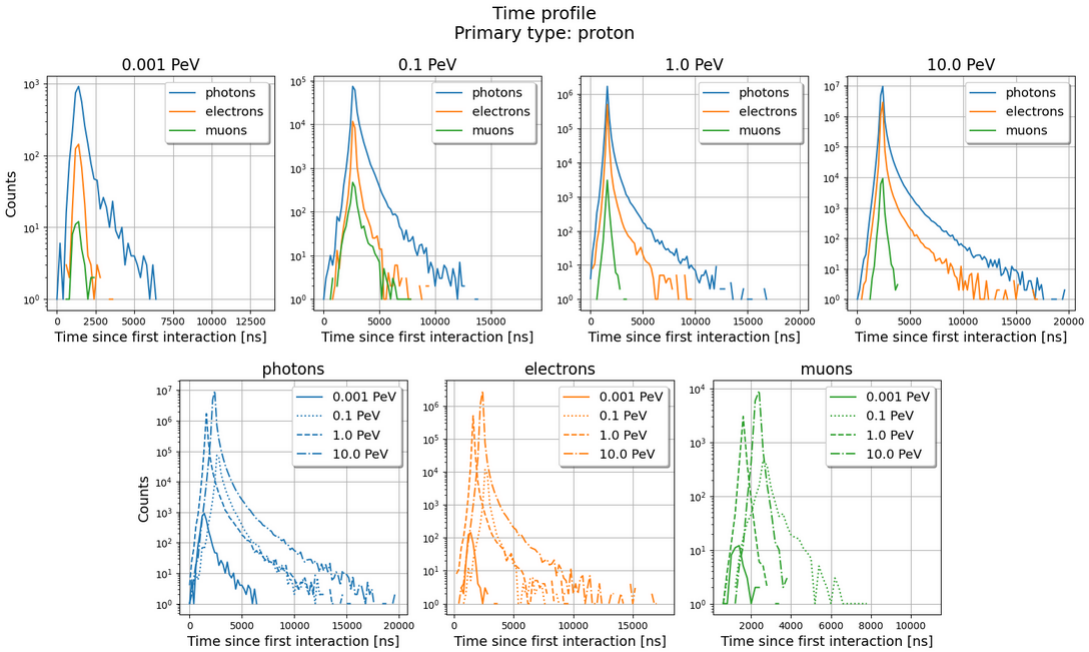

Figure 2.10: Time profile for showers initiated by protons with initial energy of 1 TeV, 100 TeV, 1 PeV and 10 PeV.

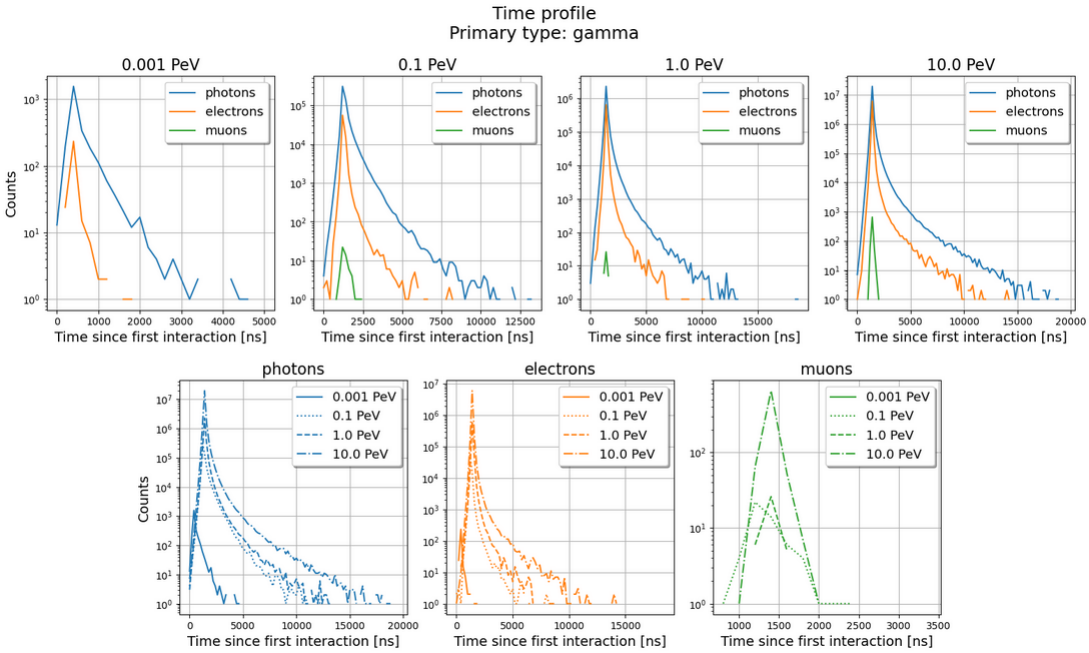

Figure 2.11: Time profile for showers initiated by gamma-rays with initial energy of 1 TeV, 100 TeV, 1 PeV and 10 PeV.

3. Conclusions

This thesis shows the importance of equipping the water Cherenkov detectors of the future SWGO observatory with a system for counting muons in order to distinguish the background from the signal. As has been seen, the density of muons represents the fundamental discriminant for understanding the nature of the detected event.

It was also shown that there is a need to take into account other factors, such as the density of photons and electrons in order not to risk confusing events of a different nature with a similar expected number of muons.

3.1 Outlook

The future of this work lies in the implementation of the array of detectors in the analysis. The detectors do not completely cover the entire area dedicated to the observatory, so only the particles passing through them can be detected. Furthermore, the efficiency and the misidentification rate of detectors must be considered, because not all particles passing through the tanks leave a strong enough signal to be seen or a signal that is interpreted correctly. It must also be taken into account that cascades do not always fall in the center of the array but can instead fall anywhere in the area and that they do not always arrive vertically but also tilted. Finally, one could extract from the gamma and proton events, for each energy separately, a statistical test that discriminates the two classes.

Another promising methodology is the use of machine learning techniques to learn directly from data and create powerful tools to build complex models for specific tasks such as gamma/hadron separation.

In general, dealing with this type of problem is not at all trivial, and the strategies that can be used are many and with different degrees of complexity and depth. But the realization of such an ambitious scientific experiment requires many years of preparation in order to be done in the best possible way, to allow us to answer some questions and, hopefully, make us come up with more.

Bibliography

[Aha+21] F. Aharonian et al. “Observation of the Crab Nebula with LHAASO-KM2A - a performance study”. In: *Chinese Physics C* 45.2 (Feb. 2021), p. 025002. DOI: 10.1088/1674-1137/abd01b. URL: https://doi.org/10.1088%5C%2F1674-1137%5C%2Fabd01b.

[Alm21] Ulisses Barres de Almeida and. “The Southern Wide-Field Gamma-ray Observatory”. In: *Astronomische Nachrichten* 342.1-2 (Jan. 2021), pp. 431–437. DOI: 10.1002/asna.202113946. URL: https://doi.org/10.1002%5C%2Fasna.202113946.

[AMP08] Alessandro De Angelis, Oriana Mansutti, and Massimo Persic. “Very-high energy gamma astrophysics”. In: *La Rivista del Nuovo Cimento* 31.4 (July 2008), pp. 187–245. ISSN: 0393697X, 0393697X. DOI: 10.1393/ncr/i2008-10032-2. URL: https://doi.org/10.1393/ncr/i2008-10032-2.

[Cao+21] Zhen Cao et al. “Ultrahigh-energy photons up to 1.4 petaelectronvolts from 12 gamma-Ray Galactic Sources”. In: *Nature* 594 (2021), pp. 33–36. DOI: 10.1038/s41586-021-03498-z. URL: https://doi.org/10.1038/s41586-021-03498-z.

[Con+21] Rúben Conceição et al. “Gamma/hadron discrimination using a small-WCD with four PMTs”. In: *Proceedings of 37th International Cosmic Ray Conference — PoS(ICRC2021)*. Vol. 395. 2021, p. 707. DOI: 10.22323/1.395.0707.

[Dor09] Michele Doro. “Novel Reflective Elements and Indirect Dark Matter Searches for MAGIC II and Future IACTs”. PhD thesis. Università degli studi di Padova, 2009. URL: http://hdl.handle.net/11577/3425635.

[Hec] Dieter (IKP) Heck. *Corsika*. URL: https://www.iap.kit.edu/corsika/.

[Hin21] Jim Hinton. “The Southern Wide-field Gamma-ray Observatory: Status and Prospects”. In: (2021). DOI: 10.48550/ARXIV.2111.13158. URL: https://arxiv.org/abs/2111.13158.

[Kun21] Samridha Kunwar. “Double-layered Water Cherenkov Detector for SWGO”. In: *Proceedings of 37th International Cosmic Ray Conference — PoS(ICRC2021)*. Vol. 395. 2021, p. 902. DOI: 10.22323/1.395.0902.

[Noe] Maximilian Noethe. *CTA-observatory/pycorsikaio: Python reader for corsika binary file format*. URL: https://github.com/cta-observatory/pycorsikaio.

[PS19] R. D. Parsons and H. Schoorlemmer. “Systematic differences due to high energy hadronic interaction models in air shower simulations in the 100 GeV-100 TeV range”. In: *Physical Review D* 100.2 (July 2019). DOI: 10.1103/physrevd.100.023010. URL: https://doi.org/10.1103%2Fphysrevd.100.023010.

[Sin09] G Sinnis. “Air shower detectors in gamma-ray astronomy”. In: *New Journal of Physics* 11.5 (May 2009), p. 055007. DOI: 10.1088/1367-2630/11/5/055007. URL: https://doi.org/10.1088/1367-2630/11/5/055007.

[SWG22] SWGO. *The Southern Wide-field Gamma-ray Observatory (SWGO)*. https://www.swgo.org/SWGOWiki/doku.php?id=start. 2019 (accessed August 15, 2022).